Theory of metastability in discrete-time open quantum dynamics

Yuan-De Jin,[1,*] Chu-Dan Qiu,[2,*] and Wen-Long Ma[2,3,†]

[1]*Department of Applied Physics, University of Science and Technology Beijing, Beijing 100083, China*

[2]*State Key Laboratory of Superlattices and Microstructures, Institute of Semiconductors, Chinese Academy of Sciences, Beijing, 100083, China*

[3]*Center of Materials Science and Opto-Electronic Technology, University of Chinese Academy of Sciences, Beijing 100049, China*

(Received 4 January 2024; accepted 18 March 2024; published 8 April 2024)

Metastability in open system dynamics describes the phenomena of initial relaxation to long-lived metastable states before decaying to the asymptotic stable states. It has been found in continuous-time stochastic dynamics of both classical and quantum systems. However, many cases of open quantum system dynamics are intrinsically discrete, and the evolution within each discrete time interval is described by an arbitrary quantum channel, which often cannot be generated by continuous-time master equations. Here we develop a general theory of metastability in discrete-time open quantum dynamics, described by sequential repetitive quantum channels. We apply the general metastability theory to a typical class of quantum channels on a target system, induced by an ancilla qubit with a pure-dephasing coupling to the target system and under Ramsey sequences. Interesting metastable behaviors are predicted and numerically demonstrated by decomposing the average dynamics of sequential quantum channels into stochastic trajectories. We also present examples of applications in quantum state and dynamics engineering of a target quantum system with an ancilla qubit.

DOI: 10.1103/PhysRevA.109.042204

I. INTRODUCTION

Metastability, ubiquitous in interacting or open systems, arises when the system dynamics settles into long-lived states before ultimately decaying to true equilibria. Previous studies found metastability in various nonequilibrium phenomena, such as phase transitions in finite-size systems [1–4] and glassy dynamics of quantum many-body systems [5–12]. Metastability also emerges in classical stochastic dynamics when there is a separation of relaxation timescales due to a spectrum splitting in the generator of the master equations [13–16].

By extending metastability from classical stochastic dynamics to the quantum domain, quantum metastability theory has been formulated for continuous-time Markovian dynamics [17–21], described mostly by Lindblad master equations [22,23]. The manifold of metastable states is argued to be composed of disjoint states, decoherence-free subspaces, and noiseless subsystems [17]. With this theoretical framework, quantum metastability has been found in various settings, such as dissipative phase transitions of the quantum Ising model [24], dynamics of quantum systems coupled to dissipative bosonic modes [25], the driven-dissipative setting of quantum spin model [26], Rabi model [27], Bose-Hubbard model [28] and long-range interacting systems [29], and experiments of Rydberg gases [30]. Other novel phenomena include metastable discrete time-crystalline phases in Floquet open systems [31–33] and Majorana bosons in metastable quadratic Markovian dynamics [34].

While current works on quantum metastability mainly concern continuous-time open quantum dynamics, many quantum processes have a discrete nature, such that the whole process is composed of a chain of discrete evolutions. Each discrete evolution can be induced by a general quantum channel, which, in many cases, cannot be generated by continuous-time master equations. The discrete-time open quantum dynamics appears in a broad range of scenarios, such as quantum random walks [35], quantum collision models [36], and quantum channel simulations [37–41]. Such processes can be described by sequential quantum channels [see Fig. 1(a)], also called discrete-time quantum Markov chains [42–45]. It remains largely unexplored whether metastability can occur for such discrete-time open quantum dynamics.

In this paper, we formulate a general theory of metastability in sequential repetitive quantum channels and derive the conditions for observing metastability. The theory is based on spectrally decomposing a quantum channel and classifying its eigenvalues. The key finding is to predict interesting metastability behaviors for sequential quantum channels on a target system induced by sequential Ramsey interferometry measurements (RIMs) of an ancilla qubit system [46,47], which is a common protocol in quantum information processing [48]. We confirm the theoretical analysis by decomposing the average dynamics of sequential channels into stochastic trajectories with Monte Carlo simulations of practical examples. The findings provide a theoretical foundation for recent experiments in polarizing a quantum environment with an ancilla qubit in solid-state systems [49–52].

*These authors contributed equally to this work.

†wenlongma@semi.ac.cn

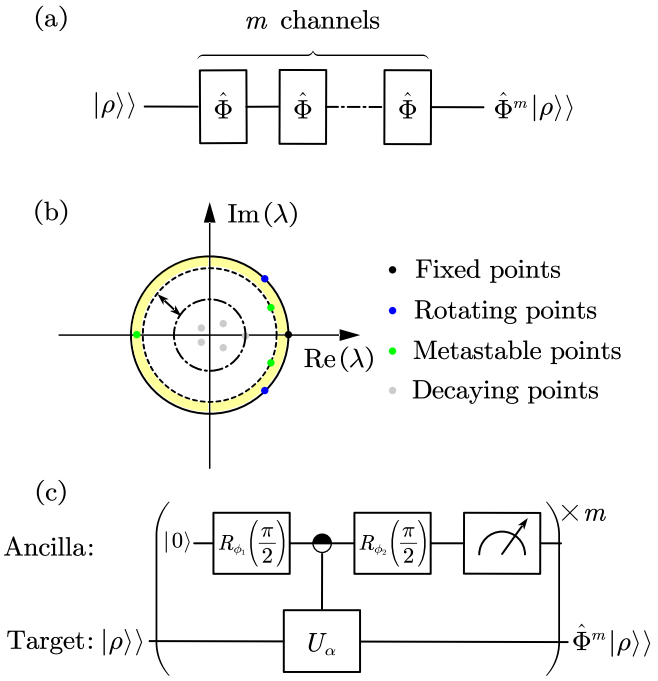

FIG. 1. (a) Schematic of sequential quantum channels. For an initial state $|\rho\rangle\rangle$ of a target system, its final state becomes $\hat{\Phi}^m|\rho\rangle\rangle$ after applying the quantum channel for m times. (b) The eigenvectors of a quantum channel can be divided into three categories: the fixed points with eigenvalue $\lambda = 1$, rotating points with $\lambda = e^{i\varphi}$ ($\varphi \neq 0$), and decaying points with $|\lambda| < 1$. The decaying points with $|\lambda| \approx 1$ are also called metastable points. Note that the complex eigenvalues of a quantum channel always come in conjugate pairs. The area shaded in yellow labels a metastable region and quantum metastability emerges when the gap (represented by an arrow) between the smallest eigenvalue in this region and the next smaller one outside the region is relatively large. (c) Schematic of the quantum circuit for sequential RIMs, where $R_\phi(\theta) = e^{-i(\cos\phi\sigma_q^x + \sin\phi\sigma_q^y)\theta/2}$ is the ancilla rotation operator and $U_\alpha = e^{-i[(-1)^\alpha B+\gamma C]t}$ is a unitary operator of the target system conditioned on the ancilla state $|\alpha\rangle_q$ ($\alpha = 0, 1$).

II. MODEL FOR METASTABILITY IN SEQUENTIAL QUANTUM CHANNELS

We first present a general model for quantum metastability in sequential quantum channels, which can be regarded as a generalization of the continuous-time framework in [17] to the discrete-time case. However, the extension is nontrivial since the channel in each cycle is not necessarily the integration of a Lindblad generator within a small time step ($\hat{\Phi} = e^{\hat{\mathcal{L}}t}$) and can be quite arbitrary (e.g., highly non-Markovian [53–55]).

The quantum channel is a completely positive and trace-preserving (CPTP) map [56–59] (see Appendix A 1 for details), which maps a density operator to another one by $\Phi(\rho) = \rho'$. One can represent a quantum channel in the Kraus representation as [56] (see Appendix A 2 a)

$$\Phi(\cdot) = \sum_\alpha M_\alpha(\cdot)M_\alpha^\dagger = \sum_\alpha \mathcal{M}_\alpha(\cdot), \tag{1}$$

where $\{M_\alpha\}$ are a set of Kraus operators satisfying $\sum_\alpha M_\alpha^\dagger M_\alpha = \mathbb{I}$ with $(\cdot)^\dagger$ denoting the Hermitian conjugation and $\mathbb{I}$ being the identity operator, and $\mathcal{M}_\alpha(\cdot) = M_\alpha(\cdot)M_\alpha^\dagger$ is a superoperator. The set of operators $\{M_\alpha^\dagger M_\alpha\}$ form a positive operator-valued measure (POVM) representing a generalized measurement, which can also be simulated by projective measurements and postselection [60–63].

The quantum channel also has a natural representation in the Hilbert-Schmidt (HS) space [59,64] (see Appendix A 2 c). A linear operator on a Hilbert space is transformed to a ket in the HS space $A = \sum_{ij} a_{ij}|i\rangle\langle j| \leftrightarrow |A\rangle\rangle = \sum_{ij} a_{ij}|ij\rangle\rangle$, and the inner product in the HS space is defined as $\langle\langle A|B\rangle\rangle = \mathrm{Tr}(A^\dagger B)$. Then a superoperator on the Hilbert space corresponds to a linear operator on the HS space: $X(\cdot)Y \to X \otimes Y^T|\cdot\rangle\rangle$, so that $\hat{\mathcal{M}}_\alpha = M_\alpha \otimes M_\alpha^*$ and $\hat{\Phi} = \sum_\alpha \hat{\mathcal{M}}_\alpha$, where $(\cdot)^T$ and $(\cdot)^*$ denote the matrix transposition and matrix conjugation, respectively. Note that we add hats on operators acting on the HS space.

Since the natural representation of a quantum channel is a linear operator on the HS space, it can be spectrally decomposed as [58]

$$\hat{\Phi} = \sum_i \lambda_i |R_i\rangle\rangle\langle\langle L_i|, \tag{2}$$

where $\lambda_i = |\lambda_i|e^{i\varphi_i}$ is the ith eigenvalue and $|R_i\rangle\rangle(|L_i\rangle\rangle)$ is the corresponding right (left) eigenvector, satisfying $\hat{\Phi}|R_i\rangle\rangle = \lambda_i|R_i\rangle\rangle$, $\hat{\Phi}^\dagger|L_i\rangle\rangle = \lambda_i^*|L_i\rangle\rangle$, and the biorthonormalization condition $\langle\langle L_i|R_j\rangle\rangle = \mathrm{Tr}(L_i^\dagger R_j) = \delta_{ij}$ with δ_{ij} being the Kronecker delta. Here we assume that the channel is diagonalizable (see Appendix A 3 for a general Jordan decomposition of a channel).

The eigenvalues $\{\lambda_i\}$ of a quantum channel are all located within a unit disk of the complex plane [56], and we order them by decreasing modulus, $|\lambda_i| \geqslant |\lambda_{i+1}|$ [Fig. 1(b)]. The eigenvectors with eigenvalue 1 are called *fixed points* [65,66], those with eigenvalue $e^{i\varphi}$ ($\varphi \neq 0$) are *rotating points* [67], and those with $|\lambda_i| < 1$ are *decaying points*. The HS subspace spanned by the fixed points and rotating points are called the asymptotic subspace (also known as the peripheral or attractor subspace). For the HS subspace spanned by the fixed points, we can always find a basis $\{|\rho_{\mathrm{fix}}^i\rangle\rangle\}$, such that $\{\rho_{\mathrm{fix}}^i\}$ are all positive operators with unit trace [$\mathrm{Tr}(\rho_{\mathrm{fix}}^i) = 1$ for any i] and orthogonal supports ($\rho_{\mathrm{fix}}^i \rho_{\mathrm{fix}}^j = 0$ if $i \neq j$) [66]. For this paper, of particular interest are the decaying points with eigenvalue $|\lambda_i| \approx 1$ called *metastable points*.

For a channel $\hat{\Phi}$ with an asymptotic subspace spanned by n fixed points, quantum metastability can emerge when there is also a metastable HS subspace spanned by $l - n$ metastable points. After sequentially applying the quantum channel for m times, we have [68]

$$\begin{aligned}\hat{\Phi}^m|\rho\rangle\rangle &= \sum_{i=1}^n c_i\big|\rho_{\mathrm{fix}}^i\big\rangle\big\rangle + \sum_{j=n+1}^l c_j\lambda_j^m|R_j\rangle\rangle + \cdots \\ &\simeq \sum_{i=1}^n c_i\big|\rho_{\mathrm{fix}}^i\big\rangle\big\rangle + \sum_{j=n+1}^l c_j e^{m(\ln|\lambda_j| + i\varphi_j)}|R_j\rangle\rangle,\end{aligned} \tag{3}$$

with $\lambda_j = |\lambda_j|e^{i\varphi_j}$ and $c_j = \langle\langle L_j|\rho\rangle\rangle = \mathrm{Tr}(L_j^\dagger\rho)$. The eigenvalues of a quantum channel can appear in conjugate pairs, i.e., for an eigenvalue $\lambda_j = |\lambda_j|e^{i\varphi_j}$ with $|R_j\rangle\rangle$ and c_j, we have $\lambda_{j+1} = |\lambda_j|e^{-i\varphi_j}$ with $|R_{j+1}\rangle\rangle = |R_j^\dagger\rangle\rangle$ and $c_{j+1} = c_j^*$.

Then we let $c'_j = |c_j|\cos(m\varphi_j + \delta_j)$, $c'_{j+1} = |c_{j+1}|\sin(m\varphi_j + \delta_j)$, $|R'_j\rangle\rangle = |R_j\rangle\rangle + |R_{j+1}\rangle\rangle$ and $|R'_{j+1}\rangle\rangle = i(|R_j\rangle\rangle - |R_{j+1}\rangle\rangle)$ with $\delta_j = \arg(c_j)$, so Eq. (3) becomes

$$\hat{\Phi}^m|\rho\rangle\rangle \simeq \sum_{i=1}^{n} c_i\big|\rho^i_{\rm fix}\big\rangle\big\rangle + \sum_{j=n+1}^{l} c'_j(m)|R'_j\rangle\rangle. \tag{4}$$

For real eigenvalues, $c'_j = c_j$ and $|R'_j\rangle\rangle = |R_j\rangle\rangle$, then $\hat{\Phi}^m|\rho\rangle\rangle \simeq \sum_{i=1}^{n} c_i|\rho^i_{\rm fix}\rangle\rangle + \sum_{j=n+1}^{l} c_j|R_j\rangle\rangle$, which is independent of m.

The contributions of the metastable points to the evolution in Eq. (4) cannot be neglected when $m \ll \mu' = 1/|\ln|\lambda_l||$, while the contribution of the other decaying points decays fast as m grows and can be omitted when $m \gg \mu'' = 1/|\ln|\lambda_{l+1}||$ [17]. So μ' and μ'' delimit a metastable region

$$\frac{1}{|\ln|\lambda_{l+1}||} \ll m \ll \frac{1}{|\ln|\lambda_l||}, \tag{5}$$

where l denotes the total dimension of the asymptotic subspace and metastable subspace. In such a region, the metastable points with real eigenvalues act like fixed points, and those with complex eigenvalues act like rotating points.

A metastable state can be fully determined by $(c_2, \ldots, c_n, c'_{n+1} \ldots, c'_l)$ [69], corresponding to a point in a $(l-1)$-dimensional HS subspace. However, $|R'_j\rangle\rangle$ is not a physical state since the trace of decaying points is zero, i.e., $\mathrm{Tr}(R'_j) = 0$ (see Appendix A 3). So we should transform the above HS subspace to a metastable state subspace, where an arbitrary metastable state is a convex combination of l disjoint extreme metastable states (EMSs) [16] (see Appendix C 1). Suppose that $\{\rho_v\}$ is the set of EMSs, then sequential channels in the metastable region can be approximated as (see Appendix C 2)

$$\hat{\Phi}^m \simeq \sum_{v=1}^{l} |\rho_v\rangle\rangle\langle\langle P_v|, \tag{6}$$

where $\{P_v\}$ is a set of positive operators satisfying $\langle\langle P_v|\rho_u\rangle\rangle = \delta_{vu}$ and $\sum_v P_v = \mathbb{I}$. Thus $\hat{\Phi}^m|\rho\rangle\rangle \simeq \sum_{v=1}^{l} p_v|\rho_v\rangle\rangle$ with $p_v = \mathrm{Tr}(P_v\rho)$ satisfying $\sum_v p_v = 1$.

When $m \gtrsim \mu'$, the contribution of the second term in Eq. (4) decreases exponentially as m increases, so the system gradually leaks from metastable states and relaxes toward the stationary states corresponding to the fixed points.

III. METASTABILITY FOR SEQUENTIAL RIMS

Then we apply the general metastability theory in the last section to a typical setting of sequential quantum channels, where the channel on a target quantum system is induced by an ancilla qubit under RIM sequences [Fig. 1(c)]. The RIM of a qubit is a common protocol to measure the qubit decoherence [70,71] or to detect a signal in quantum sensing [48,72]. Recently, such a protocol was extended to engineer or purify the state of a target system coupled to a qubit [49–52]. Suppose that the target system is coupled to an ancilla qubit by a pure-dephasing Hamiltonian as

$$H = \sigma^z_q \otimes B + \gamma\, \mathbb{I}_q \otimes C, \tag{7}$$

where σ^i_q is the Pauli-i operator of the ancilla, B and C are both operators on the target system, and γ controls the magnitude of the second term [73].

In a single RIM, an ancilla qubit is initialized to $|0\rangle_q$ and rotated to $|\psi\rangle_q = R_{\phi_1}(\frac{\pi}{2})|0\rangle_q = (|0\rangle_q - ie^{i\phi_1}|1\rangle_q)/\sqrt{2}$, with the rotation operator being $R_\phi(\theta) = e^{-i(\cos\phi\sigma^x_q + \sin\phi\sigma^y_q)\theta/2}$, then interacts with the target system under the Hamiltonian H for time t, undergoes another rotation $R_{\phi_2}(\frac{\pi}{2})$ and is finally projectively measured in the basis $\{|0\rangle_q, |1\rangle_q\}$. The measurement result is either 0 or 1 for a single RIM.

Such a process induces a quantum channel on the target system, which can be written in Stinespring representation as [74] (see Appendix A 2 b)

$$\Phi(\rho) = \mathrm{Tr}_q[U(\rho_q \otimes \rho)U^\dagger], \tag{8}$$

where $\rho_q = |\psi\rangle_q\langle\psi|$ and $U = e^{-iHt} = \sum_{\alpha=0,1} |\alpha\rangle_q\langle\alpha| \otimes U_\alpha$ with $U_\alpha = e^{-i[(-1)^\alpha B + \gamma C]t}$. By tracing over the ancilla qubit, we get the natural representation

$$\hat{\Phi} = \hat{\mathcal{M}}_0 + \hat{\mathcal{M}}_1 = (\hat{\mathcal{U}}_0 + \hat{\mathcal{U}}_1)/2, \tag{9}$$

where $\hat{\mathcal{U}}_\alpha = U_\alpha \otimes U^*_\alpha$, and $\hat{\mathcal{M}}_\alpha = M_\alpha \otimes M^*_\alpha$ with the Kraus operator $M_\alpha = [U_0 - (-1)^\alpha e^{i\Delta\phi}U_1]/2$ and $\Delta\phi = \phi_1 - \phi_2$. Note that the channel above depends on the initial state of the ancilla and describes non-Markovian open quantum dynamics, which cannot be generated by continuous-time master equations.

The channel induced by RIM [Eq. (9)] is a unital mixed-unitary channel [59,75,76], satisfying $\Phi(\mathbb{I}) = \mathbb{I}$. It has been proven that ρ is a fixed point of a unital channel if and only if it commutes with every Kraus operator [59], i.e., $[\rho, M_\alpha] = 0$ for any α. When $\gamma \neq 0$, the fixed points of the channel [Eq. (9)] depend on the commutativity of B and C (see Appendix B for the proof).

(i) If $[B, C] = 0$, then B and C can be diagonalized simultaneously, $B = \sum_{j=1}^{d} b_j|j\rangle\langle j|$ and $C = \sum_{j=1}^{d} c_j|j\rangle\langle j|$, so the fixed points must include the set of rank-1 projections $\{|j\rangle\langle j|\}_{j=1}^{d}$ and their linear combinations, with d denoting the dimension of Hilbert space $\mathcal{H}$ of the target system.

(ii) If $[B, C] \neq 0$, B and C can be reduced simultaneously to a block-diagonal form by a unitary transformation W, $B = W(\bigoplus_{j=1}^{r} B_j)W^\dagger$ and $C = W(\bigoplus_{j=1}^{r} C_j)W^\dagger$, where W is chosen such that B_j and C_j for any j cannot be reduced further to have more blocks. Such a block diagonalization partitions the Hilbert space of the target system $\mathcal{H}$ into the direct sum of r subspaces $\mathcal{H} = \bigoplus_{j=1}^{r} \mathcal{H}_j$, and $[B_j, C_j] \neq 0$ for at least one subspace $\mathcal{H}_j$ with $\dim(\mathcal{H}_j) \geqslant 2$. Then the fixed points must include the set of projection operators $\{\Pi_j\}_{j=1}^{r}$ $(r < d)$ and their linear combinations, where Π_j is the projection to the subspace $\mathcal{H}_j$, satisfying $\sum_{j=1}^{r} \Pi_j = \mathbb{I}$.

Sequential RIMs of the ancilla induce sequential quantum channels on the target system. Thus, for $[B, C] = 0$, the asymptotic operation of sequential such channels is a polarizing channel (or a projective measurement) on the target system [77–80], while for $[B, C] \neq 0$ it can be a depolarizing channel at least for the subspace $\mathcal{H}_j$ with $\dim(\mathcal{H}_j) \geqslant 2$. Interestingly, if we consider the ancilla dynamics, the target system causes decoherence of the ancilla, and these two cases correspond exactly to those where the target system produces static thermal or dynamical quantum noise, respectively [81–84].

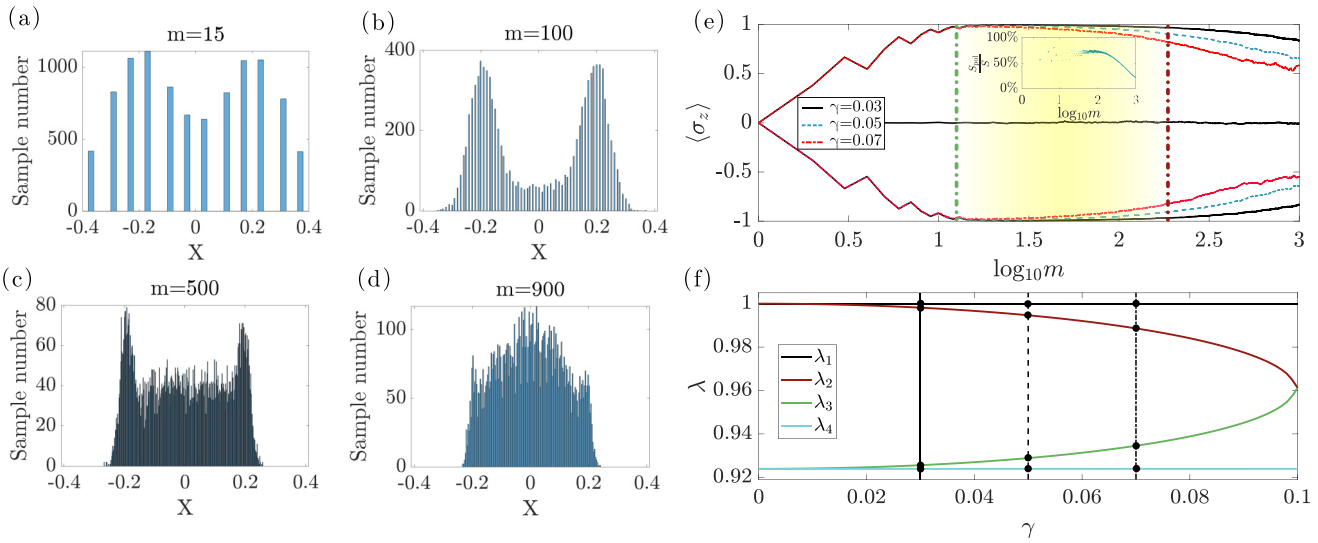

FIG. 2. Metastability in sequential RIMs of an ancilla qubit coupled to a single target qubit. (a)–(d) Measurement statistics of sequential RIMs from Monte Carlo simulations (with $\gamma = 0.05$), where we present four stages of evolutions of measurement polarization statistics. (a) When m is relatively small, the width of peaks is large and the two peaks have overlaps. (b) For a larger m, quantum metastability emerges and there appears two well-distinguished distribution peaks corresponding to two EMSs. (c) The two peaks gradually disappear as m increases beyond the metastable region. (d) Finally, there appears a single peak corresponding to the maximally mixed state $\mathbb{I}/2$ when $m \gg \mu'$. (e) $\langle\sigma_z\rangle$ of the target qubit for three classes of trajectories in Monte Carlo simulations with different γ: the target qubit is either polarized to nearly $|0\rangle$ (upper lines) or $|1\rangle$ (lower lines), or depolarized to $\mathbb{I}/2$ (black line in the middle). The metastable region of the case that $\gamma = 0.05$ is marked with a gradient yellow shade. The boundaries of the region ($\mu'' = 1/|\ln|\lambda_3||$ and $\mu' = 1/|\ln|\lambda_2||$) are calculated by numerically diagonalizing the channel [also see (f), the gap emerges between λ_2 and λ_3] and are labeled with maroon (dark gray) and green (light gray) dotted dash vertical lines. Inset: Proportion of samples in polarized regions to total samples (also for $\gamma = 0.05$). (f) Spectrum of the channel on the target system as a function of γ, where the spectra corresponding to γ in (e) are labeled. All the simulations contains 10^4 samples with $\Delta\phi = \pi/2$.

As the open system dynamics described by Lindblad master equations can be unraveled with quantum trajectories [85,86], the average dynamics of sequential quantum channels can also be decomposed into stochastic trajectories

$$\hat{\Phi}^m = (\hat{\mathcal{M}}_0 + \hat{\mathcal{M}}_1)^m = \sum_{\alpha_1,\alpha_2\ldots,\alpha_m=0}^{1} \hat{\mathcal{M}}_{\alpha_m}\ldots\hat{\mathcal{M}}_{\alpha_2}\hat{\mathcal{M}}_{\alpha_1}, \tag{10}$$

with the probability to obtain each trajectory being $p(\alpha_1,\alpha_2\ldots,\alpha_m) = \langle\langle\mathbb{I}|\hat{\mathcal{M}}_{\alpha_m}\ldots\hat{\mathcal{M}}_{\alpha_2}\hat{\mathcal{M}}_{\alpha_1}|\rho\rangle\rangle = \mathrm{Tr}\,[\mathcal{M}_{\alpha_m}(\cdots\{\mathcal{M}_{\alpha_2}[\mathcal{M}_{\alpha_1}(\rho)]\})]$.

So for m repetitive RIMs, the measurement results of the ancilla will be a sequence of m binary numbers $(\alpha_1,\alpha_2,\ldots,\alpha_m)$ with $\alpha_i \in \{0,1\}$, inducing an operation $\hat{\mathcal{M}}_{\alpha_m}\ldots\hat{\mathcal{M}}_{\alpha_2}\hat{\mathcal{M}}_{\alpha_1}$ on the target system (note that $[\hat{\mathcal{M}}_0,\hat{\mathcal{M}}_1] \neq 0$ if $[B,C] \neq 0$). Denote the number of 0/1 as m_0/m_1 ($m_0+m_1=m$), one can get a measurement frequency $F = \{m_0/m, m_1/m\}$. The measurement polarization $X = (m_0-m_1)/(2m)$ denotes the different classes of stochastic trajectories that the target system undergoes [79,80]. The measurement distribution of X can show multiple distribution peaks, with each peak corresponding to a fixed point of the channel. The measurement statistics of such trajectories for commuting Kraus operators have been exactly derived in [79,80], and the case for non-commuting Kraus operators is rather complicated and will be studied in a future work [87]. In both cases, the measurement statistics can be efficiently obtained by Monte Carlo simulations [79,88].

Metastability can occur when $[B,C] \neq 0$ and γ is small. When $\gamma = 0$, we show above that the fixed points $\{|j\rangle\langle j|\}_{j=1}^d$ span a d-dimensional asymptotic subspace. When γ is small, γC is a perturbation on B, and the d-dimensional asymptotic state subspace breaks down into a r-dimensional asymptotic subspace (spanned by the fixed points $\{\Pi_j\}_{j=1}^r$) and another $(d-r)$-dimensional metastable state subspace, which corresponds to $n=r$ and $l=d$ in Eq. (4). The EMSs for this case are $\{|j\rangle\langle j|\}_{j=1}^d$ up to some corrections (see Appendix C). Then, the metastable polarization of the target system occurs when $1/|\ln|\lambda_{d+1}|| \ll m \ll 1/|\ln|\lambda_d||$, which can also be seen in the measurement statistics of the ancilla qubit.

IV. EXAMPLES

We consider several examples of sequential RIMs with different target systems. First, consider that the target system is a single qubit with $B=\sigma_z$ and $C=\sigma_x$, then obviously $[B,C] \neq 0$. With the target qubit initially in a maximally mixed state $\mathbb{I}/2$, we show the polarization statistics of sequential RIMs by Monte Carlo simulations in Fig. 2. For a small γ, there appear two distinguishable peaks corresponding to two EMSs as m increases to the metastable region [Figs. 2(a) and 2(b)]. While beyond that region, the above two peaks gradually vanish and there appears a single peak corresponding to the stable state $\mathbb{I}/2$ [Figs. 2(c) and 2(d)]. The polarization plateau in the evolution of $\langle\sigma_z\rangle$ clearly shows the metastability [Fig. 2(e)], where the target qubit is polarized to $|0\rangle$ or $|1\rangle$ (eigenstates of $B=\sigma_z$) apart from some

corrections. The metastable regions [Fig. 2(e)] agree with those predicted by the spectrum of the channel [Fig. 2(f)]. In numerical simulations, we classify the Monte Carlo samples into three categories by $X \in [-0.5, -0.15)$, $[-0.15, 0.15]$ or (0.15,0.5], where $[-0.5, -0.15)$ and (0.15,0.5] are polarization ranges and $[-0.15, 0.15]$ is a depolarization range. For each m, the data in Fig. 2(e) are obtained by averaging over all the samples of single categories (note that the percentage of polarized samples also shows metastable plateau). EMSs here can be represented as $\rho_{1,2} = \mathbb{I}/2 + c_2^{M,m} R_2/h$, where c_2^M (c_2^m) is the maximal (minimal) eigenvalue of L_2, and $h = \sqrt{\langle\langle L_2|L_2\rangle\rangle\langle\langle R_2|R_2\rangle\rangle}$ is a normalization coefficient (see Appendix C for details).

Then we consider a target system composed of multiple qubits, such as multiple ^{13}C nuclear spins coupled to a nitrogen vacancy (NV) center electron spin (as an ancilla) [89,90]. In this system, the NV center interacts with K nuclear spins through hyperfine interaction $B = \sum_{k=1}^{K} \boldsymbol{A}_k \cdot \boldsymbol{I}_k$, where $\boldsymbol{A}_k = (A_k^x, A_k^y, A_k^z)$ and $\boldsymbol{I}_k = (I_k^x, I_k^y, I_k^z)$. The free Hamiltonian of the target system is the dipolar interaction between nuclear spins $C = \sum_{j<k} D_{jk}[\boldsymbol{I}_j \cdot \boldsymbol{I}_k - \frac{3(\boldsymbol{I}_j \cdot \boldsymbol{r}_{jk})(\boldsymbol{I}_k \cdot \boldsymbol{r}_{jk})}{r_{jk}^2}]$ ($\gamma = 1$), where D_{jk} denotes the dipolar coupling strength, and $\boldsymbol{r}_{jk}$ is the displacement from the jth to the kth target spin. Typically $[B, C] \neq 0$ [90], and the only fixed point is the maximally mixed state $\mathbb{I}/2^K$. Since the nuclear dipolar interaction is much smaller than the hyperfine interaction, i.e., $D_{jk} \ll |\boldsymbol{A}_k|$, there will be 2^K EMSs, forming a $(2^K - 1)$-dimensional metastable state subspace. For measurement statistics of sequential RIMs, there will be 2^K peaks if $\mu'' \ll m \ll \mu'$, which collapse to a single peak corresponding to $\mathbb{I}/2^K$ as $m \gtrsim \mu'$ (see Appendix D 1 for simulations).

Metastability theory still applies when the ancilla is under sequential dynamical decoupling (DD) control [91,92]. For periodic DD sequences and nearly independent nuclear spins, we have $B = \sum_{k=1}^{K} A_k^{\perp} I_k^{\perp}$, $\quad C = \Delta_\omega \sum_{k=1}^{K} I_k^z$ ($\gamma = 1$), where $A_k^{\perp} = \sqrt{(A_k^x)^2 + (A_k^y)^2}$ and $I_k^{\perp} = \cos\xi I_k^x + \sin\xi I_k^y$ with $\xi = \arctan(A_k^y/A_k^x)$, and $\Delta_\omega = \omega_L - \omega_T$ denotes the detuning of DD frequency ω_L relative to the nuclear Larmor frequency ω_T. When ω_L resonates with ω_T, C can be tuned to zero [93], leading to the polarization of the nuclear spins [51]. If $\omega_L \neq \omega_T$, the nuclear spins are generally depolarized since $[B, C] \neq 0$, but if Δ_ω is small (relative to $A_k^{\perp}$), the nuclear spins can still be polarized for a metastable region of m (see Appendix D 2 for simulations). Moreover, in all the above examples, numerical simulations show that quantum metastability is quite robust even if the target systems suffers additional noise (see Appendix E).

V. CONCLUSION AND OUTLOOK

We extend the quantum metastability theory from the continuous-time open quantum dynamics described by Lindblad master equations to the discrete-time open quantum dynamics described by sequential general quantum channels. We consider the quantum channel induced by both RIM and DD sequences of an ancilla qubit. Metastable polarization behaviors are demonstrated by numerical simulations for a quantum system containing single or multiple qubits. Our work provides theoretical support for quantum state and dynamics engineering with sequential measurement and control of an ancilla system.

In this paper, we focus on the channels generated by RIMs evolving with the Hamiltonian [Eq. (7)], where the metastable state subspace includes only EMSs. It will be interesting for future topics to consider more general channels, whose fixed points as a kind of preserved information may include decoherence-free subspaces or noiseless subsystems [94,95]. In the presence of control imperfection or environmental noise, the channel should be slightly perturbed from the ideal ones and the preserved information may become metastable, and we expect that the metastability theory in this paper can provide a useful guide to make full use of such metastablely preserved information.

ACKNOWLEDGMENTS

We thank Ryusuke Hamazaki for helpful discussions. The research is supported by the National Natural Science Foundation of China (Grants No. 12174379 and No. E31Q02BG), the Chinese Academy of Sciences (Grants No. E0SEBB11 and No. E27RBB11), the Innovation Program for Quantum Science and Technology (Grant No. 2021ZD0302300), and the Chinese Academy of Sciences Project for Young Scientists in Basic Research (Grant No. YSBR-090).

APPENDIX A: FUNDAMENTALS OF QUANTUM CHANNELS

1. Definition of quantum channels

Denote the linear operators acting on a Hilbert space $\mathcal{H}$ as $\mathcal{B}(\mathcal{H})$, then a map $\Phi : \mathcal{B}(\mathcal{H}) \to \mathcal{B}(\mathcal{H})$ is a quantum channel if it satisfies the following conditions [58].

(1) Linear map: For any $A, B \in \mathcal{B}(\mathcal{H})$ and complex number c, $\Phi(A + cB) = \Phi(A) + c\Phi(B)$.

(2) Completely positive (CP): For any positive operator σ, $(\Phi \otimes \mathbb{I})(\sigma)$ is still a positive operator, with $\mathbb{I}$ being the identity operator on an additional system with dimension $\dim(\mathcal{H})$ and σ being a density matrix for the composite system.

(3) Trace preserving (TP): For any $A \in \mathcal{B}(\mathcal{H})$, $\mathrm{Tr}[\Phi(A)] = \mathrm{Tr}(A)$. This implies unitality of $\Phi^\dagger$, i.e., $\Phi^\dagger(\mathbb{I}) = \mathbb{I}$, where $\Phi^\dagger$ is defined by $\mathrm{Tr}[B\Phi(A)] = \mathrm{Tr}[\Phi^\dagger(B)A]$.

So a quantum channel is a CPTP map, which describes the most general quantum evolution that a quantum system undergoes.

2. Representations of quantum channels

Every quantum channel has four different representations [59]: the Kraus representation, the Stinespring representation, the natural representation, and the Choi representation. In this paper, we use the first three representations of quantum channels.

a. Kraus representation

Of the four representations, the Kraus representation is the most commonly used one. In this representation, a quantum channel is fully characterized by a collection of Kraus

operators $\{M_\alpha\}_{\alpha=1}^r$ satisfying $\sum_\alpha M_\alpha^\dagger M_\alpha = \mathbb{I}$ so that

$$\Phi(\cdot) = \sum_{\alpha=1}^{r} M_\alpha(\cdot)M_\alpha^\dagger = \sum_{\alpha=1}^{r} \mathcal{M}_\alpha(\cdot), \tag{A1}$$

where $\mathcal{M}_\alpha(\cdot) = M_\alpha(\cdot)M_\alpha^\dagger$ is a superoperator.

For a given quantum channel, the set of Kraus operators can be chosen with some degree of freedom under unitary transformations. For convenience, we define

$$\mathbf{M} = \begin{bmatrix} M_1 \\ \vdots \\ M_r \end{bmatrix}, \tag{A2}$$

then $\mathbf{M}^\dagger\mathbf{M} = \mathbb{I}$. By inserting a $r \times r$ unitary operator T, we have $\mathbf{M}^\dagger T^\dagger T\mathbf{M} = \mathbf{M}'\mathbf{M}' = \mathbb{I}$, with $\mathbf{M}' = T\mathbf{M}$. Then $\mathbf{M}'$ and $\mathbf{M}$ are Kraus operators of the same quantum channel since

$$\begin{aligned} \Phi'(\cdot) &= \sum_{\alpha=1}^{r} M'_\alpha(\cdot)M'^\dagger_\alpha \\ &= \sum_{\alpha,\beta,\gamma=1}^{r} T_{\alpha\beta}M_\beta(\cdot)T^*_{\alpha\gamma}M_\gamma^\dagger \\ &= \sum_{\beta,\gamma=1}^{r} \delta_{\gamma\beta}M_\beta(\cdot)M_\gamma^\dagger \\ &= \sum_{\beta=1}^{r} M_\beta(\cdot)M_\beta^\dagger = \Phi(\cdot). \end{aligned} \tag{A3}$$

Note that $T_{\alpha\beta}$ is the matrix element of the unitary matrix T, so $\sum_{\alpha=1}^r T^*_{\alpha\gamma}T_{\alpha\beta} = \delta_{\gamma\beta}$.

b. Stinespring representation

The stinespring representation is a dilation of a quantum channel. The dilation can be realized by coupling the target system to an ancilla system, and letting the composite system undergo a unitary evolution and then tracing over the ancilla system

$$\Phi(\rho) = \mathrm{Tr}_a[U(\rho_a \otimes \rho)U^\dagger], \tag{A4}$$

where ρ_a is the initial state of the ancilla system and U is a unitary of the composite system and Tr_a denotes the trace over the ancilla system. For an r-dimensional ancilla system with an orthonormal basis $\{|\alpha\rangle_a\}_{\alpha=1}^r$ and an initial state $\rho_a = |1\rangle_a\langle 1|$, the Kraus operator can be easily obtained as $M_\alpha = \langle r|U|1\rangle_a$. The freedom in choosing the Kraus operators corresponds to the freedom in choosing the orthonormal basis of the ancilla when taking the partial trace in Eq. (A4). For a new basis $\{T^\dagger|\alpha\rangle_a\}_{\alpha=1}^r$ with T being a unitary operator, the Kraus operators are changed to a new set $\{M'_\alpha\}_{\alpha=1}^r$, with $M'_\alpha = \sum_{\beta=1}^r T_{\alpha\beta}M_\beta$, but the quantum channel remains unchanged.

c. Natural representation

For sequential applications of the same channel, it is convenient to use the natural representation of a quantum channel. To understand this representation, we need to introduce the HS space. In the HS space, an operator on a d-dimensional Hilbert space (represented by a $d \times d$ matrix) is transformed to a $d^2 \times 1$ vector

$$A = \begin{bmatrix} a_{11} & \dots & a_{1d} \\ \vdots & \ddots & \vdots \\ a_{d1} & \dots & a_{dd} \end{bmatrix} = \begin{bmatrix} \boldsymbol{a}_1 \\ \vdots \\ \boldsymbol{a}_d \end{bmatrix} \Rightarrow |A\rangle\rangle = \begin{bmatrix} \boldsymbol{a}_1^T \\ \vdots \\ \boldsymbol{a}_d^T \end{bmatrix}, \tag{A5}$$

where $\boldsymbol{a}_i^T$ is the transpose of $\boldsymbol{a}_i$. Such a transformation can also be represented by $A = \sum_{ij} a_{ij}|i\rangle\langle j| \Rightarrow |A\rangle\rangle = \sum_{ij} a_{ij}|ij\rangle\rangle$ with $|ij\rangle\rangle = |i\rangle \otimes |j\rangle$. The inner product in the HS space is defined as

$$\begin{aligned} \langle\langle A|B\rangle\rangle &= \sum_{ijpq} a^*_{ij}b_{pq}\langle\langle ij|pq\rangle\rangle \\ &= \sum_{ij} a^*_{ij}b_{ij} \\ &= \sum_{j} (A^\dagger B)_{jj} \\ &= \mathrm{Tr}(A^\dagger B). \end{aligned} \tag{A6}$$

Then a superoperator (defined by $\mathcal{O}(\rho) = A\rho B$) becomes a single matrix $A \otimes B^T$ acting on a vector $|\rho\rangle\rangle$ in HS space

$$A\rho B = \sum_{ijpq} a_{ij}\rho_{jp}b_{pq}|i\rangle\langle q| \;\Rightarrow\; A \otimes B^T\,|\rho\rangle\rangle, \tag{A7}$$

so the natural representation of the channel in Eq. (A1) in HS space is

$$\hat{\Phi} = \sum_{\alpha=1}^{r} \hat{\mathcal{M}}_\alpha, \tag{A8}$$

where $\hat{\mathcal{M}}_\alpha = M_\alpha \otimes M^*_\alpha$. Note that we add hats on the operators acting on the HS space to distinguish them from the corresponding superoperators acting on the operator space of the quantum system.

3. Jordan decomposition of a quantum channel

The natural representation of a quantum channel on the HS space is a $d^2 \times d^2$ square operator. This operator may not be diagonalizable, but can always be converted to a Jordan normal form as

$$\begin{aligned} \hat{\Phi} &= S\left(\bigoplus_{k=1}^{\kappa} \mathcal{J}_{d_k}(\lambda_k)\right)S^{-1} \\ &= S\left(\sum_{|\lambda_j|=1} \lambda_j\mathcal{P}_j + \sum_{|\lambda_k|<1} (\lambda_k\mathcal{P}_k + \mathcal{N}_k)\right)S^{-1}, \end{aligned} \tag{A9}$$

where S is an invertible $d^2 \times d^2$ matrix, κ is the total number of Jordan blocks, and $\mathcal{J}_{d_i}(\lambda_i)$ represents a d_i-dimensional Jordan block corresponding to the eigenvalue λ_i, $\mathcal{P}_j$ is a projection operator, and $\mathcal{N}_k$ is a nilpotent operator satisfying $\mathcal{N}_{k=1}^{d_k} = 0$. Considering that $\sum_{k=1}^{\kappa} d_k = d$, then the channel is diagonalizable iff $\kappa = d$. Note that the Jordan blocks corresponding to the fixed points or rotating points (with eigenvalues $|\lambda_i| = 1$) are all rank-1 projectors [96].

If the channel is diagonalizable, we have

$$\hat{\Phi} = \sum_i \lambda_i|R_i\rangle\rangle\langle\langle L_i|, \tag{A10}$$

where $\{|R_i\rangle\rangle, |L_i\rangle\rangle\}$ is a complete biorthogonal basis satisfying $\langle\langle L_i|R_j\rangle\rangle = \delta_{ij}$. Since a quantum channel is a CPTP map, one can prove that the spectral radius of the channel is 1, i.e., all eigenvalues of that lie in the unit disk of the complex plane [58]. The TP property of $\hat{\Phi}$ also implies the unitality of $\hat{\Phi}^\dagger$, i.e., $\hat{\Phi}^\dagger|\mathbb{I}\rangle\rangle = |\mathbb{I}\rangle\rangle$ or there exists a left eigenvector $\langle\langle\mathbb{I}|$ for eigenvalue 1, then for the right eigenvectors corresponding to $\lambda_j \neq 1$ (including both the rotating points and decaying points), we have

$$\langle\langle\mathbb{I}|R_j\rangle\rangle = \mathrm{Tr}(R_j) = 0. \tag{A11}$$

Moreover, the complex eigenvalues always come in conjugate pairs of complex numbers since a quantum channel is a Hermiticity-preserving map (due to its CP property), i.e., $\Phi(A^\dagger) = \Phi(A)^\dagger$. For an eigenmatrix A with eigenvalue λ, we have $\Phi(A^\dagger) = \Phi(A)^\dagger = \lambda^* A^\dagger$. So $A^\dagger$ is another eigenmatrix with eigenvalue λ^*.

4. Sequential quantum channels with rotating points

If the channel has n_0 fixed points, $n - n_0$ rotating points, and $l - n$ metastable points, then after sequentially applying the quantum channel for m times, we have

$$\begin{aligned}\hat{\Phi}^m|\rho\rangle\rangle &= \sum_{i=1}^{n_0} c_i \left|\rho_{\mathrm{fix}}^i\right\rangle\rangle + \sum_{j=n_0+1}^{n} c_j \lambda_j^m \left|R_{\mathrm{rot}}^j\right\rangle\rangle \\ &\quad + \sum_{k=n+1}^{l} c_k \lambda_k^m |R_k\rangle\rangle + \cdots \\ &\simeq \sum_{i=1}^{n_0} c_i \left|\rho_{\mathrm{fix}}^i\right\rangle\rangle + \sum_{j=n_0+1}^{n} c_j e^{im\varphi_j} \left|R_{\mathrm{rot}}^j\right\rangle\rangle \\ &\quad + \sum_{k=n+1}^{l} c_k e^{m(\ln|\lambda_k| + i\varphi_k)} |R_k\rangle\rangle, \end{aligned} \tag{A12}$$

where we truncate the equation as in Eq. (3) of the main text.

Then, in the metastable region, by considering conjugate pairs of complex eigenvalues and absorbing the phase into c, we have

$$\hat{\Phi}^m|\rho\rangle\rangle \simeq \sum_{i=1}^{n_0} c_i \left|\rho_{\mathrm{fix}}^i\right\rangle\rangle + \sum_{j=n_0+1}^{l} c'_j(m)|R'_j\rangle\rangle, \tag{A13}$$

where c'_j is similarly defined as in Eq. (4) of the main text. Note that that the second term in Eq. (A13) includes both rotating points and metastable points. Then in the construction of EMSs and metastable states, we may consider the contributions of both fixed points and rotating points. For the examples in this paper, the channels induced RIMs often have no rotating points.

APPENDIX B: FIXED POINTS OF THE CHANNEL INDUCED BY RIMs

Now we consider the fixed points of the quantum channel on a target system induced by a RIM of an ancilla qubit. The ancilla is coupled to the target system with a pure-dephasing Hamiltonian

$$H = \sigma_q^z \otimes B + \gamma\, \mathbb{I}_q \otimes C, \tag{B1}$$

where σ_q^i is the Pauli-i operator of the ancilla, B and C are both operators on the target system and γ controls the magnitude of the second term. For a RIM, the Kraus representation of the channel on the target system is

$$\hat{\Phi} = \hat{\mathcal{M}}_0 + \hat{\mathcal{M}}_1 = (\hat{\mathcal{U}}_0 + \hat{\mathcal{U}}_1)/2, \tag{B2}$$

where $\hat{\mathcal{U}}_\alpha = U_\alpha \otimes U_\alpha^*$ with $U_\alpha = e^{-i[(-1)^\alpha B + \gamma C]}$, and $\hat{\mathcal{M}}_\alpha = M_\alpha \otimes M_\alpha^*$ with the Kraus operator $M_\alpha = [U_0 - (-1)^\alpha e^{i\Delta\phi} U_1]/2$ and $\Delta\phi = \phi_1 - \phi_2$. Then the fixed points induced by such a unital channel is given by the following proposition.

Proposition 1. The fixed points of the channel in Eq. (B2) depends on the commutativity of B and C. If $[B, C] = 0$, the fixed points must include the linear combinations of rank-1 projections $\{|j\rangle\langle j|\}_{j=1}^d$; if $[B, C] \neq 0$, the fixed points must include the linear combinations of projection operators $\{\Pi_j\}_{j=1}^r$ ($r < d$), satisfying $\sum_{j=1}^r \Pi_j = \mathbb{I}$.

Proof. It is proven that ρ is a fixed point of a unital channel if and only if it commutes with every Kraus operator [59], i.e., $[\rho, M_\alpha] = 0$ for any α. This implies that $[\rho, U_0] = [\rho, U_1] = 0$. If the above condition is always satisfied for any α, then $[\rho, B] = [\rho, C] = 0$.

If $[B, C] = 0$, then B and C can be diagonalized simultaneously, $B = \sum_{j=1}^d b_j|j\rangle\langle j|$ and $C = \sum_{j=1}^d c_j|j\rangle\langle j|$. So the fixed points must include the rank-1 projections $\{|j\rangle\langle j|\}_{j=1}^d$ and their linear combinations.

If $[B, C] \neq 0$, we can simultaneously block diagonalize them by a unitary transformation

$$B = W\left(\bigoplus_{j=1}^r B_j\right)W^\dagger, \quad C = W\left(\bigoplus_{j=1}^r C_j\right)W^\dagger, \tag{B3}$$

where $r \leqslant d$ is the number of blocks (with equality occurring only when $[B, C] = 0$ and all of blocks are one-dimensional), W is a unitary matrix and should be chosen such that B_j and C_j for any j cannot be reduced further to have more blocks. Such a block diagonalization partitions the Hilbert space of the target system into a direct sum of r subspaces $\mathcal{H} = \bigoplus_{j=1}^r \mathcal{H}_j$, with $WB_jW^\dagger$ and $WC_jW^\dagger$ being operators acting on $\mathcal{H}_j$. Since $[B, C] \neq 0$, we have $[B_j, C_j] \neq 0$ for at least one subspace $\mathcal{H}_j$ with $\dim(\mathcal{H}_j) \geqslant 2$. Thus the Kraus operator is also transformed to a block-diagonal form as $M_\alpha = \bigoplus_{j=1}^r M_\alpha^j$. Then the fixed points must include the set of projections $\{\Pi_j\}_{j=1}^r$ ($r \leqslant d$) and their linear combinations, where Π_j is the projector to $\mathcal{H}_j$.

Now we prove that there are no other fixed points for the case $[B, C] \neq 0$, where there is at least one block with $[B_j, C_j] \neq 0$ and $[M_0^j, M_1^j] \neq 0$. Suppose there is another density matrix satisfying $[\rho', M_\alpha^j] = 0$. If $\mathrm{rank}\rho' = d_j$, then $[\rho', M_0^j] = [\rho', M_1^j] = 0$. Since the positive operator ρ' can be diagonalized, this implies that $[M_0^j, M_1^j] = 0$. If $\mathrm{rank}(\rho') < d_j$, then we formulates another fixed point $\rho'' = \rho' + \eta\mathbb{I}$ with η being a positive number such that $\mathrm{rank}(\rho'') = d_j$, and the proof is similar to the previous case.

APPENDIX C: QUANTUM METASTABILITY IN SEQUENTIAL RIMS FOR A TARGET QUBIT

1. Construction of EMSs

If target system is a single qubit with $B = \sigma_z$ and $C = 0$, the fixed points are spanned by $|00\rangle\rangle$ and $|11\rangle\rangle$, where $\{|0\rangle, |1\rangle\}$ are eigenstates of σ_z. When there exists a small perturbing Hamiltonian $\gamma C = \gamma\sigma_x$, the channel has a single fixed point $|\rho_{\rm fix}\rangle\rangle = |\mathbb{I}\rangle\rangle/2$, and a metastable point $|R_2\rangle\rangle$. So the dimension of the metastable state subspace is $2 - 1 = 1$. Assume that λ_2 is real, then R_2 and L_2 can be chosen to be Hermitian [17]. Suppose that $L_2 = c_2^M|M\rangle\langle M| + c_2^m|m\rangle\langle m|$ with c_2^M (c_2^m) being the maximum (minimum) eigenvalue and $\{|M\rangle, |m\rangle\}$ forming a orthonormal basis, then the EMSs can be constructed as

$$\begin{aligned} |\rho_1\rangle\rangle &= |\rho_{\rm fix}\rangle\rangle + (c_2^M/h)|R_2\rangle\rangle, \\ |\rho_2\rangle\rangle &= |\rho_{\rm fix}\rangle\rangle + (c_2^m/h)|R_2\rangle\rangle, \end{aligned} \tag{C1}$$

where $h = \sqrt{\langle\langle L_2|L_2\rangle\rangle\langle\langle R_2|R_2\rangle\rangle}$ is a normalization coefficient that will be derived below.

We require that ρ_1 and ρ_2 are pure states, then $\mathrm{Tr}(\rho_1^2) = \mathrm{Tr}(\rho_2^2) = 1$, so

$$\begin{aligned} 1 = \mathrm{Tr}(\rho_1^2) &= \mathrm{Tr}\left[\mathbb{I}^2/4 + \left(c_2^M/h\right)R_2 + \left(c_2^M/h\right)^2 R_2^2\right] \\ &= 1/2 + \left(c_2^M/h\right)^2 \mathrm{Tr}\left(R_2^2\right) \\ &\Downarrow \\ 1/2 &= \left(c_2^M/h\right)^2 \mathrm{Tr}\left(R_2^2\right). \end{aligned} \tag{C2}$$

We can derive a similar expression from $\mathrm{Tr}(\rho_2^2) = 1$, i.e., $1/2 = (c_2^m/h)^2\mathrm{Tr}(R_2^2)$, so

$$\begin{aligned} h^2 &= \left[\left(c_2^M\right)^2 + \left(c_2^m\right)^2\right]\mathrm{Tr}\left(R_2^2\right) \\ &= \mathrm{Tr}\left(L_2^2\right)\mathrm{Tr}\left(R_2^2\right) \\ &= \langle\langle L_2|L_2\rangle\rangle\langle\langle R_2|R_2\rangle\rangle. \end{aligned} \tag{C3}$$

We illustrate the above analysis with a simple example. Consider a fixed point $|\rho_{\rm fix}\rangle\rangle = |\mathbb{I}\rangle\rangle/2 = (|00\rangle\rangle + |11\rangle\rangle)/2$, and a metastable point with $|R_2\rangle\rangle = (|00\rangle\rangle - |11\rangle\rangle)/2$, then $|L_2\rangle\rangle = |00\rangle\rangle - |11\rangle\rangle$, where $c_2^M = 1$, $c_2^m = -1$, and $h = 1$. Thus the EMSs are

$$\begin{aligned} |\rho_1\rangle\rangle &= |\rho_{\rm fix}\rangle\rangle + |R_2\rangle\rangle = |00\rangle\rangle, \\ |\rho_2\rangle\rangle &= |\rho_{\rm fix}\rangle\rangle - |R_2\rangle\rangle = |11\rangle\rangle. \end{aligned} \tag{C4}$$

For general cases, the EMSs are the eigenstates of B up to some corrections.

2. Construction of arbitrary metastable states

Any metastable state can be represented by a convex combination of EMSs,

$$|\rho_{\rm MS}\rangle\rangle = p_1|\rho_1\rangle\rangle + p_2|\rho_2\rangle\rangle, \tag{C5}$$

where $p_{1,2} = \langle\langle P_1|\rho\rangle\rangle = \mathrm{Tr}(P_{1,2}\rho)$ with $P_{1,2}$ being observables satisfying $\langle\langle P_v|\rho_u\rangle\rangle = \delta_{vu}$, $P_1 + P_2 = \mathbb{I}$, and $P_{1,2} \geqslant 0$. Below we show how to construct such observables.

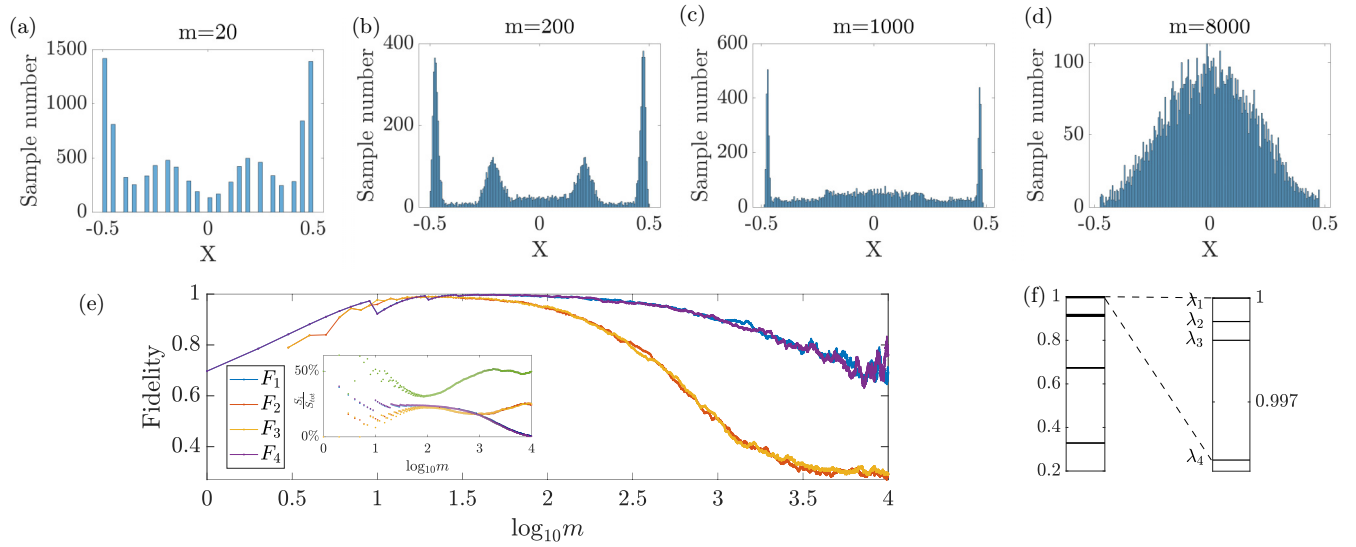

FIG. 3. Metastability in sequential RIMs of an ancilla qubit coupled to two target spins with zero magnetic field. (a)–(d) Measurement statistics of sequential RIMs from Monte Carlo simulation for two target qubits, in which we present four stages of the system evolution. (a) When the time of measurements m is small, the different peaks are not fully distinguishable due to the large distribution width. (b) For larger m, the four peaks corresponding to four EMSs can be well distinguished. (c) The peaks corresponding to the two EMSs ($|22\rangle\rangle$ and $|33\rangle\rangle$) disappear, while those relevant to $|11\rangle\rangle$ and $|44\rangle\rangle$ still remain. (d) All the peaks are merged into a single one corresponding to the only fixed point. (e) The trajectory of evolution of fidelity. Upper lines are F_1 and F_4, decreasing more slowly than the lower lines showing F_2 and F_3, which indicates faster vanishing of EMSs relevant to $|22\rangle\rangle$ and $|33\rangle\rangle$. Inset: The proportion of samples corresponding to each trajectory and the green (uppermost) dot represents the proportion of samples except for four trajectories. (f) Spectra of the quantum channel. In all Monte Carlo simulations, we use 10^4 samples and the parameters are $\Delta\phi = \pi/2$, $|\mathbf{A}_1| = 0.585\,\mathrm{kHz}$, $|\mathbf{A}_2| = 0.890\,\mathrm{kHz}$, $|D_{12}| = 11.6\,\mathrm{Hz}$, and $||C||/||B|| = 0.0316$.

Since $|\rho_{\rm MS}\rangle\rangle = \Phi^m|\rho\rangle\rangle$ in the metastable region $\mu'' \ll m \ll \mu'$, so we have

$$\Phi^m \simeq |\rho_1\rangle\rangle\langle\langle P_1| + |\rho_2\rangle\rangle\langle\langle P_2|. \tag{C6}$$

Comparing the above equation with $\Phi^m \simeq \frac{1}{2}|\mathbb{I}\rangle\rangle\langle\langle\mathbb{I}| + |R_2\rangle\rangle\langle\langle L_2|$ in the metastable region, we have

$$\begin{aligned}\frac{1}{2}|\mathbb{I}\rangle\rangle\langle\langle\mathbb{I}| + |R_2\rangle\rangle\langle\langle L_2| &= \left(\frac{1}{2}|\mathbb{I}\rangle\rangle + \frac{c_2^M}{h}|R_2\rangle\rangle\right)\langle\langle P_1| \\ &\quad + \left(\frac{1}{2}|\mathbb{I}\rangle\rangle + \frac{c_2^m}{h}|R_2\rangle\rangle\right)\langle\langle P_2| \\ &\Downarrow \\ |R_2\rangle\rangle\langle\langle L_2| &= \frac{c_2^M}{h}|R_2\rangle\rangle\langle\langle P_1| \\ &\quad + \frac{c_2^m}{h}|R_2\rangle\rangle(\langle\langle\mathbb{I}| - \langle\langle P_1|) \\ &= |R_2\rangle\rangle\left[\frac{c_2^M}{h}\langle\langle P_1| + \frac{c_2^m}{h}(\langle\langle\mathbb{I}| - \langle\langle P_1|)\right],\end{aligned} \tag{C7}$$

so we have

$$P_1 = \frac{hL_2 - c_2^m\mathbb{I}}{\Delta c_2}, \quad P_2 = \frac{-hL_2 + c_2^M\mathbb{I}}{\Delta c_2}, \tag{C8}$$

with $\Delta c_2 = c_2^M - c_2^m$.

APPENDIX D: QUANTUM METASTABILITY IN SEQUENTIAL QUANTUM CHANNELS FOR MULTIPLE TARGET QUBITS

In this section, we consider a practical example to show quantum metastability in sequential quantum channels, that is, an NV center electron spin (ancilla qubit) in a ^{13}C nuclear spins bath (target system). The coupling Hamiltonian is the same as Eq. (6) in the main text by taking $\gamma = 1$,

$$H = \sigma_q^z \otimes B + C, \tag{D1}$$

with

$$\begin{aligned}B &= f(t)\sum_{k=1}^{K}\boldsymbol{A}_k\cdot\boldsymbol{I}_k, \\ C &= \omega_L\sum_{k=1}^{K}I_k^z + \sum_{j<k}D_{jk}\left[\boldsymbol{I}_j\cdot\boldsymbol{I}_k - \frac{3(\boldsymbol{I}_j\cdot\boldsymbol{r}_{jk})(\boldsymbol{I}_k\cdot\boldsymbol{r}_{jk})}{r_{jk}^2}\right],\end{aligned} \tag{D2}$$

where $f(t)$ is a modulation function accounting for possible DD control of the ancilla qubit, $\boldsymbol{A}_k = (A_k^x, A_k^y, A_k^z)$ is the hyperfine interaction vector of the kth nuclear spin, $\boldsymbol{I}_k = (I_k^x, I_k^y, I_k^z)$ is the nuclear spin operator vector, $d = 2^K$ is the dimension of the Hilbert space of the target system, $\omega_L = \gamma_n B_z$ is the Larmor precession frequency of nuclear spins, $D_{jk} = \frac{\mu_0\gamma_n^2}{4\pi r_{jk}^3}$ with γ_n being the gyromagnetic ratio of the target spins and μ_0 being vacuum permeability, and $\boldsymbol{r}_{jk}$ is the displacement from the jth target spin to the kth target spin. In the simulations below we use practical parameters.

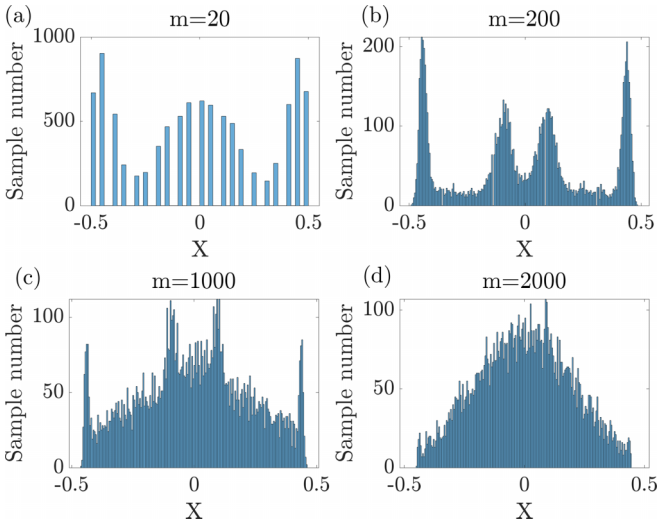

FIG. 4. Monte Carlo simulations for sequential RIMs and two target spins with a weak magnetic field. The evolution of measurement statistics can be seen from (a) to (d), which shows that the metastability theory still applies to the system with a Zeeman term. All the Monte Carlo simulations contain 10^4 samples, and the parameters are $\Delta\phi = \pi/2$, $|\mathbf{A}_1| = 0.138$ MHz, $|\mathbf{A}_2| = 0.517$ MHz, $|D_{12}| = 60.5$ Hz, $\omega_L = 13.5$ KHz, and $||C||/||B|| = 0.0412$.

1. RIM sequences

For RIM sequences, we assume that the external magnetic field is zero, so that

$$\begin{aligned}B &= \sum_{k=1}^{K}\boldsymbol{A}_k\cdot\boldsymbol{I}_k, \\ C &= \sum_{j<k}D_{jk}\left[\boldsymbol{I}_j\cdot\boldsymbol{I}_k - \frac{3(\boldsymbol{I}_j\cdot\boldsymbol{r}_{jk})(\boldsymbol{I}_k\cdot\boldsymbol{r}_{jk})}{r_{jk}^2}\right].\end{aligned} \tag{D3}$$

To show metastable polarization of nuclear spins, we calculate the following fidelity:

$$F_i(\rho) = \mathrm{Tr}\sqrt{\sqrt{\rho_i}\rho\sqrt{\rho_i}}, \tag{D4}$$

where $\rho_i = |i\rangle\langle i|$ is the ith EMS with $|i\rangle$ being the eigenstate of B ($i \in \{1, 2, 3, 4\}$), and ρ is the state obtained by averaging over the Monte Carlo samples within a specific interval of X. Here the four intervals of X are chosen as

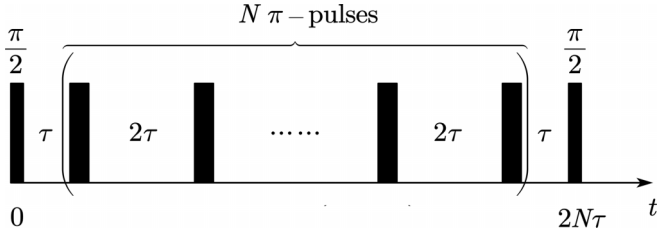

FIG. 5. Schematic of an N-pulse CPMG sequence with N $\pi-$flips at $t = \tau, 3\tau, \ldots, (2N-1)\tau$.

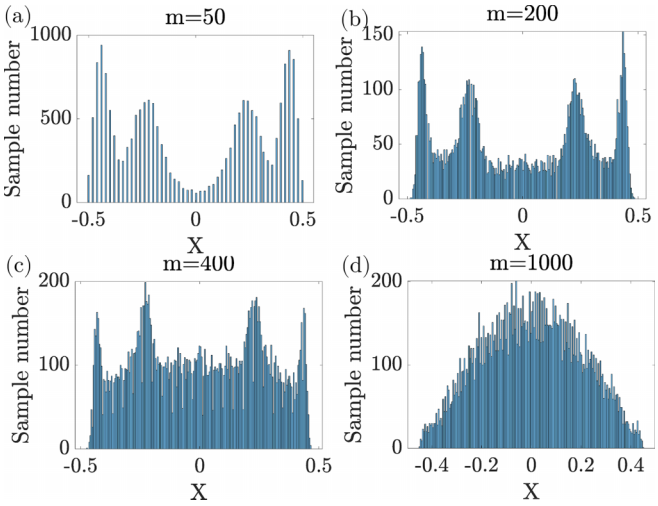

FIG. 6. Monte Carlo simulations for sequential DD sequences and two target spins. As m grows, the peaks emerge and become apparent (a), (b) since they are corresponding to the four EMSs, then they (c) vanish gradually as m approaching the boundary of metastable region, which (d) finally collapse to the maximally mixed state. All the Monte Carlo simulations contain 10^4 samples, and the parameters are $\Delta\phi = \pi/2$, $|\mathbf{A}_1| = 5\,\mathrm{kHz}$, $|\mathbf{A}_2| = 6\,\mathrm{kHz}$, $\omega_L = 135\,\mathrm{kHz}$, $\Delta_\omega = 10^{-3}\omega_L$, $N = 32$.

$[-0.5, 0.4)$, $[-0.3, 0.1)$, $[0.1, 0.3]$, $(0.4, 0.5]$. The measurement statistics and the fidelity plateaus clearly show the metastability behaviors (Fig. 3). Metastability still remains when there is a weak external magnetic field ($\omega_L \ll |\mathbf{A}_k|$) (Fig. 4).

2. DD sequences

DD sequences are a generalization of RIM sequences, with additional N π-flips of the ancilla spin during each cycle (Fig. 5). Then we have

$$B = f(t)\sum_{k=1}^{K}\boldsymbol{A}_k\cdot\boldsymbol{I}_k, \quad C = \omega_L\sum_{k=1}^{K}I_k^z, \tag{D5}$$

where $f(t)$ is the DD modulation function jumping between $+1$ and -1 every time the sensor is flipped by a DD pulse. Here for simplicity, we neglect the dipolar interaction term in C, which means these target spins are spatially far away from each other.

For N-pulse Carr-Purcell-Meiboom-Gill (CPMG) control, $f(t) = f(t+T)$ with $T = 4\tau$. Specifically, $f(t) = -1$ when $\tau + \beta T \leqslant t < 3\tau + \beta T$ with $\beta = 0, 1, \ldots, \frac{N}{2} - 1$ and $f(t) = 1$ otherwise. Then $f(t)$ can be expanded into a Fourier series as $f(t) = \sum_{n=1}^{\infty} c_n \cos(n\omega_T t)$, where c_n is nth Fourier expansion coefficient and $\omega_T = \pi/(2\tau)$ is the angular frequency. For the weak coupling condition, i.e., $|\boldsymbol{A}_k| \ll \omega_L$, we can approximate $f(t)$ by keeping only the first term in the Fourier series, $f(t) \approx c_1\cos(\omega_T t) = \frac{4}{\pi}\cos(\omega_T t)$. Then B becomes

$$B = \frac{4}{\pi}\cos(\omega_T t)\sum_{k=1}^{K}\boldsymbol{A}_k\cdot\boldsymbol{I}_k \approx \frac{4}{\pi}\cos(\omega_T t)\sum_{k=1}^{K}A_k^{\perp}I_k^{\perp}, \tag{D6}$$

where $A_k^{\perp} = \sqrt{(A_k^x)^2 + (A_k^y)^2}$ and $I_k^{\perp} = \cos\alpha I_k^x + \sin\alpha I_k^y$, and the longitude component $A_z I_z$ can be neglected in the weak coupling region [93].

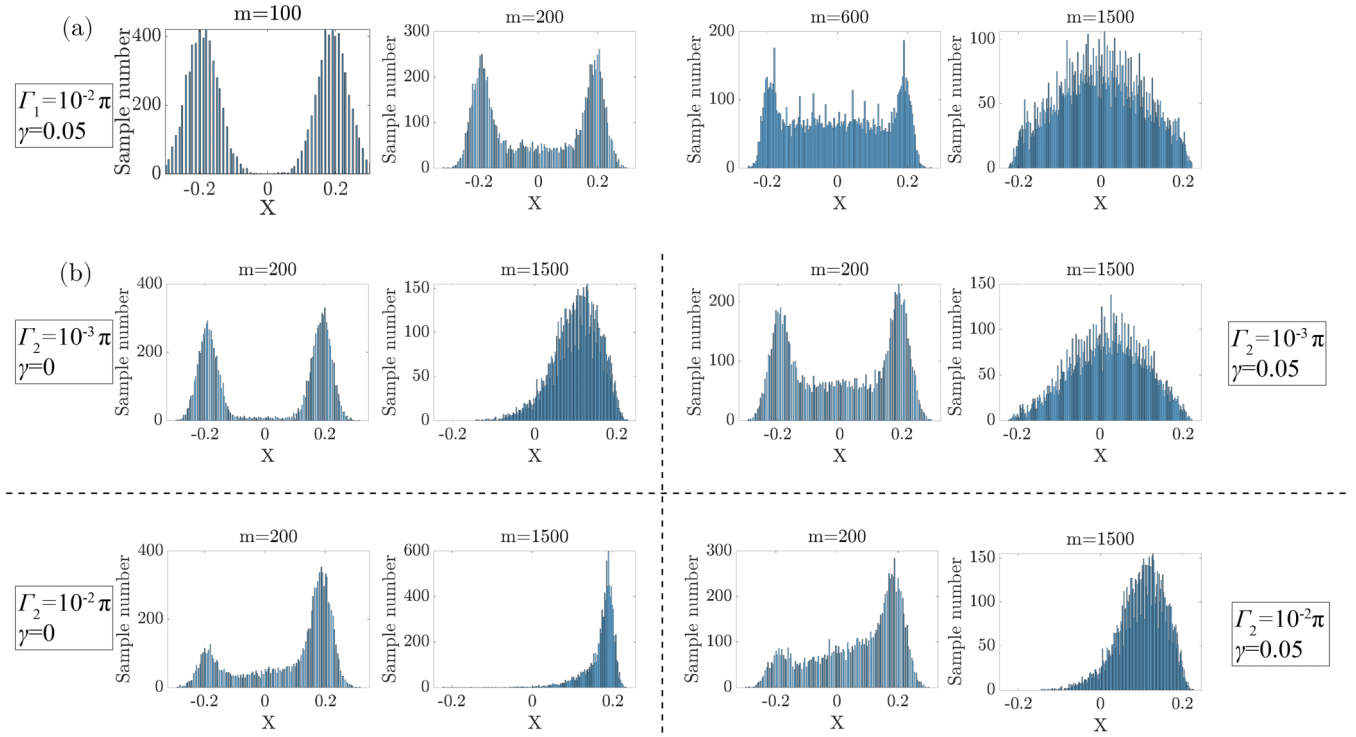

FIG. 7. Monte Carlo simulations for sequential RIMs and a single target qubit with (a) dephasing noise and (b) relaxation noise. The noise rates are shown in the figure, and the other parameters are the same as those in Fig. 2 of the main text.

Now we move to the rotating frame with respect to $\omega_T I_z$, by using rotating wave approximation, the effective Hamiltonian becomes time-independent,

$$B = \frac{2}{\pi}\sum_{k=1}^{K} A_k^{\perp} I_k^{\perp}, \quad C = \Delta_\omega \sum_{k=1}^{K} I_k^z, \tag{D7}$$

where $\Delta_\omega = \omega_L - \omega_T$ is the detuning away from the Larmor precession frequency. Then if we choose $\omega_T = \omega_L$, also called the resonance condition, then $C = 0$ and the target qubits can be polarized. However, practically speaking, the adjustment of the frequency may not be precise. With a small detuning, quantum metastability theory shows that the target can still be polarized with appropriate rounds of DD, as numerically verified in Fig. 6.

APPENDIX E: QUANTUM METASTABILITY FOR A NOISY TARGET SYSTEM

In this section, we show that quantum metastability is robust even when the target system suffers additional noise. Suppose that the target system (a single qubit) suffers dephasing and relaxation noise, the evolution of the composite systems can be described by the following Lindblad master equation:

$$\frac{\mathrm{d}\rho_{\mathrm{tot}}}{\mathrm{d}t} = -i[H, \rho_{\mathrm{tot}}] + \sum_k \Gamma_k \left(L_k \rho_{\mathrm{tot}} L_k^\dagger - \frac{1}{2}\{L_k^\dagger L_k, \rho_{\mathrm{tot}}\} \right), \tag{E1}$$

where ρ_{tot} is the density matrix of the composite system, $H = \sigma_z \otimes B + \gamma\, \mathbb{I}_q \otimes C$, $L_1 = \sigma_z$ denotes the target dephasing, $L_2 = \sigma_- = |1\rangle\langle 0|$ denotes the target relaxation, and Γ_k is the noise rate.

We perform Monte Carlo simulations for each kind of dissipation separately. The results show that the dephasing noise of the target system does not influence the measurement statistics and metastability behaviors [see Fig. 7(a)]. However, with the relaxation of the target system, the peak corresponding to the fixed point $|00\rangle\rangle$ (when $\gamma = 0$) or the EMS perturbed from $|00\rangle\rangle$ (when $\gamma \neq 0$) is gradually transferred to the other peak as m increases. Nevertheless, metastability still occurs if the relaxation rate is very small or when m is relatively small [see Fig. 7(b)].

[1] B. Gaveau and L. S. Schulman, Theory of nonequilibrium first-order phase transitions for stochastic dynamics, J. Math. Phys. **39**, 1517 (1998).

[2] B. Gaveau, A. Lesne, and L. Schulman, Spectral signatures of hierarchical relaxation, Phys. Lett. A **258**, 222 (1999).

[3] J. C. Boettger and D. C. Wallace, Metastability and dynamics of the shock-induced phase transition in iron, Phys. Rev. B **55**, 2840 (1997).

[4] P. W. Anderson, *Basic Notions of Condensed Matter Physics*, 1st ed., edited by P. W. Anderson (CRC Press, Boca Raton FL, 2018).

[5] K. Binder and A. P. Young, Spin glasses: Experimental facts, theoretical concepts, and open questions, Rev. Mod. Phys. **58**, 801 (1986).

[6] J. Jäckle and S. Eisinger, A hierarchically constrained kinetic Ising model, Z. Phys. B: Condens. Matter **84**, 115 (1991).

[7] P. Sollich and M. R. Evans, Glassy time-scale divergence and anomalous coarsening in a kinetically constrained spin chain, Phys. Rev. Lett. **83**, 3238 (1999).

[8] L. F. Cugliandolo and G. Lozano, Real-time nonequilibrium dynamics of quantum glassy systems, Phys. Rev. B **59**, 915 (1999).

[9] J. P. Garrahan and D. Chandler, Geometrical explanation and scaling of dynamical heterogeneities in glass forming systems, Phys. Rev. Lett. **89**, 035704 (2002).

[10] P. Sollich and M. R. Evans, Glassy dynamics in the asymmetrically constrained kinetic Ising chain, Phys. Rev. E **68**, 031504 (2003).

[11] G. Biroli and J. P. Garrahan, Perspective: The glass transition, J. Chem. Phys. **138**, 12A301 (2013).

[12] Z. Lan, M. van Horssen, S. Powell, and J. P. Garrahan, Quantum slow relaxation and metastability due to dynamical constraints, Phys. Rev. Lett. **121**, 040603 (2018).

[13] B. Gaveau and L. S. Schulman, Dynamical metastability, J. Phys. A **20**, 2865 (1987).

[14] S. Z. D. Cheng and A. Keller, The role of metastable states in polymer phase transitions: Concepts, principles, and experimental observations, Annu. Rev. Mater. Sci. **28**, 533 (1998).

[15] B. Gaveau and M. Moreau, Metastable relaxation times and absorption probabilities for multidimensional stochastic systems, J. Phys. A **33**, 4837 (2000).

[16] B. Gaveau and L. S. Schulman, Multiple phases in stochastic dynamics: Geometry and probabilities, Phys. Rev. E **73**, 036124 (2006).

[17] K. Macieszczak, M. Guţă, I. Lesanovsky, and J. P. Garrahan, Towards a theory of metastability in open quantum dynamics, Phys. Rev. Lett. **116**, 240404 (2016).

[18] M. Merkli, H. Song, and G. P. Berman, Multiscale dynamics of open three-level quantum systems with two quasi-degenerate levels, J. Phys. A: Math. Theor. **48**, 275304 (2015).

[19] K. Macieszczak, D. C. Rose, I. Lesanovsky, and J. P. Garrahan, Theory of classical metastability in open quantum systems, Phys. Rev. Res. **3**, 033047 (2021).

[20] K. Macieszczak, Operational approach to metastability, arXiv:2104.05095.

[21] C. A. Brown, K. Macieszczak, and R. L. Jack, Unravelling metastable Markovian open quantum systems, Phys. Rev. A **109**, 022244 (2024).

[22] G. Lindblad, On the generators of quantum dynamical semigroups, Commun. Math. Phys. **48**, 119 (1976).

[23] V. Gorini, A. Kossakowski, and E. C. G. Sudarshan, Completely positive dynamical semigroups of N -Level systems, J. Math. Phys. **17**, 821 (1976).

[24] D. C. Rose, K. Macieszczak, I. Lesanovsky, and J. P. Garrahan, Metastability in an open quantum Ising model, Phys. Rev. E **94**, 052132 (2016).

[25] S. B. Jäger, T. Schmit, G. Morigi, M. J. Holland, and R. Betzholz, Lindblad master equations for quantum systems coupled to dissipative bosonic modes, Phys. Rev. Lett. **129**, 063601 (2022).

[26] H. Landa, M. Schiró, and G. Misguich, Multistability of driven-dissipative quantum spins, Phys. Rev. Lett. **124**, 043601 (2020).

[27] A. Le Boité, M.-J. Hwang, and M. B. Plenio, Metastability in the driven-dissipative Rabi model, Phys. Rev. A **95**, 023829 (2017).

[28] T. Liu, Y.-R. Zhang, K. Xu, J. Cui, and H. Fan, Discrete time crystal in a driven-dissipative Bose-Hubbard model with two-photon processes, Phys. Rev. A **105**, 013710 (2022).

[29] N. Defenu, Metastability and discrete spectrum of long-range systems, Proc. Natl. Acad. Sci. USA **118**, e2101785118 (2021).

[30] F. Letscher, O. Thomas, T. Niederprüm, M. Fleischhauer, and H. Ott, Bistability versus metastability in driven dissipative Rydberg gases, Phys. Rev. X **7**, 021020 (2017).

[31] Z. Gong, R. Hamazaki, and M. Ueda, Discrete time-crystalline order in cavity and circuit QED systems, Phys. Rev. Lett. **120**, 040404 (2018).

[32] F. M. Gambetta, F. Carollo, M. Marcuzzi, J. P. Garrahan, and I. Lesanovsky, Discrete time crystals in the absence of manifest symmetries or disorder in open quantum systems, Phys. Rev. Lett. **122**, 015701 (2019).

[33] A. Cabot, F. Carollo, and I. Lesanovsky, Metastable discrete time-crystal resonances in a dissipative central spin system, Phys. Rev. B **106**, 134311 (2022).

[34] V. P. Flynn, E. Cobanera, and L. Viola, Topology by dissipation: Majorana Bosons in metastable quadratic markovian dynamics, Phys. Rev. Lett. **127**, 245701 (2021).

[35] S. Attal, F. Petruccione, C. Sabot, and I. Sinayskiy, Open quantum random walks, J. Stat. Phys. **147**, 832 (2012).

[36] F. Ciccarello, S. Lorenzo, V. Giovannetti, and G. M. Palma, Quantum collision models: Open system dynamics from repeated interactions, Phys. Rep. **954**, 1 (2022).

[37] S. Lloyd and L. Viola, Engineering quantum dynamics, Phys. Rev. A **65**, 010101(R) (2001).

[38] E. Andersson and D. K. L. Oi, Binary search trees for generalized measurements, Phys. Rev. A **77**, 052104 (2008).

[39] C. Shen, K. Noh, V. V. Albert, S. Krastanov, M. H. Devoret, R. J. Schoelkopf, S. M. Girvin, and L. Jiang, Quantum channel construction with circuit quantum electrodynamics, Phys. Rev. B **95**, 134501 (2017).

[40] J. Han, W. Cai, L. Hu, X. Mu, Y. Ma, Y. Xu, W. Wang, H. Wang, Y. P. Song, C.-L. Zou, and L. Sun, Experimental simulation of open quantum system dynamics via trotterization, Phys. Rev. Lett. **127**, 020504 (2021).

[41] W. Cai, J. Han, L. Hu, Y. Ma, X. Mu, W. Wang, Y. Xu, Z. Hua, H. Wang, Y. P. Song, J.-N. Zhang, C.-L. Zou, and L. Sun, High-efficiency arbitrary quantum operation on a high-dimensional quantum system, Phys. Rev. Lett. **127**, 090504 (2021).

[42] S. Gudder, Quantum Markov chains, J. Math. Phys. **49**, 072105 (2008).

[43] J. Guan, Y. Feng, and M. Ying, Decomposition of quantum Markov chains and its applications, J. Comput. Syst. Sci. **95**, 55 (2018).

[44] J. Novotný, J. Maryška, and I. Jex, Quantum Markov processes: From attractor structure to explicit forms of asymptotic states: Asymptotic dynamics of quantum Markov processes, Eur. Phys. J. Plus **133**, 310 (2018).

[45] D. Amato, P. Facchi, and A. Konderak, Asymptotics of quantum channels, J. Phys. A: Math. Theor. **56**, 265304 (2023).

[46] N. F. Ramsey, A molecular beam resonance method with separated oscillating fields, Phys. Rev. **78**, 695 (1950).

[47] H. Lee, P. Kok, and J. P. Dowling, A quantum Rosetta stone for interferometry, J. Mod. Opt. **49**, 2325 (2002).

[48] C. L. Degen, F. Reinhard, and P. Cappellaro, Quantum sensing, Rev. Mod. Phys. **89**, 035002 (2017).

[49] D. B. R. Dasari, S. Yang, A. Chakrabarti, A. Finkler, G. Kurizki, and J. Wrachtrup, Anti-Zeno purification of spin baths by quantum probe measurements, Nat. Commun. **13**, 7527 (2022).

[50] M. T. Mądzik, T. D. Ladd, F. E. Hudson, K. M. Itoh, A. M. Jakob, B. C. Johnson, J. C. McCallum, D. N. Jamieson, A. S. Dzurak, A. Laucht, and A. Morello, Controllable freezing of the nuclear spin bath in a single-atom spin qubit, Sci. Adv. **6**, eaba3442 (2020).

[51] G.-Q. Liu, J. Xing, W.-L. Ma, P. Wang, C.-H. Li, H. C. Po, Y.-R. Zhang, H. Fan, R.-B. Liu, and X.-Y. Pan, Single-shot readout of a nuclear spin weakly coupled to a nitrogen-vacancy center at room temperature, Phys. Rev. Lett. **118**, 150504 (2017).

[52] D. D. Bhaktavatsala Rao, S. Yang, S. Jesenski, E. Tekin, F. Kaiser, and J. Wrachtrup, Observation of nonclassical measurement statistics induced by a coherent spin environment, Phys. Rev. A **100**, 022307 (2019).

[53] A. Rivas, S. F. Huelga, and M. B. Plenio, Quantum non-Markovianity: Characterization, quantification and detection, Rep. Prog. Phys. **77**, 094001 (2014).

[54] I. de Vega and D. Alonso, Dynamics of non-Markovian open quantum systems, Rev. Mod. Phys. **89**, 015001 (2017).

[55] H.-P. Breuer, E.-M. Laine, J. Piilo, and B. Vacchini, Colloquium: Non-Markovian dynamics in open quantum systems, Rev. Mod. Phys. **88**, 021002 (2016).

[56] K. Kraus, A. Böhm, J. D. Dollard, and WH. Wootters, *States, Effects, and Operations Fundamental Notions of Quantum Theory: Lectures in Mathematical Physics at the University of Texas at Austin* (Springer, New York, 1983).

[57] F. Caruso, V. Giovannetti, C. Lupo, and S. Mancini, Quantum channels and memory effects, Rev. Mod. Phys. **86**, 1203 (2014).

[58] M. M. Wolf, Quantum Channels and Operations-Guided Tour, Lecture Notes (2012).

[59] J. Watrous, *The Theory of Quantum Information* (Cambridge University Press, Cambridge, England, 2018).

[60] M. Oszmaniec, L. Guerini, P. Wittek, and A. Acín, Simulating positive-operator-valued measures with projective measurements, Phys. Rev. Lett. **119**, 190501 (2017).

[61] M. Oszmaniec, F. B. Maciejewski, and Z. Puchała, Simulating all quantum measurements using only projective measurements and postselection, Phys. Rev. A **100**, 012351 (2019).

[62] T. Singal, F. B. Maciejewski, and M. Oszmaniec, Implementation of quantum measurements using classical resources and only a single ancillary qubit, npj Quantum Inf **8**, 82 (2022).

[63] N. Linden and P. Skrzypczyk, How to use arbitrary measuring devices to perform almost perfect measurements, arXiv:2203.02593.

[64] I. Bengtsson and K. Życzkowski, *Geometry of Quantum States: An Introduction to Quantum Entanglement* (Cambridge University Press, Cambridge, England, 2017).

[65] A. Arias, A. Gheondea, and S. Gudder, Fixed points of quantum operations, J. Math. Phys. **43**, 5872 (2002).

[66] D. Burgarth, G. Chiribella, V. Giovannetti, P. Perinotti, and K. Yuasa, Ergodic and mixing quantum channels in finite dimensions, New J. Phys. **15**, 073045 (2013).

[67] V. V. Albert, Asymptotics of quantum channels: Conserved quantities, an adiabatic limit, and matrix product states, Quantum **3**, 151 (2019).
[68] Here we assume that the channel has no rotating points, see Appendix A 4 for sequential quantum channels with rotating points.
[69] Considering that $\mathrm{Tr}(R_j) = 0$ for decaying points and $\mathrm{Tr}(\rho^i_{\mathrm{fix}}) = 1$, so $\sum_{i=1}^{n} c_i = 1$, and $c_1 = 1 - \sum_{i=2}^{n} c_i$.
[70] L. Chirolli and G. Burkard, Decoherence in solid-state qubits, Adv. Phys. **57**, 225 (2008).
[71] M. Schlosshauer, Quantum decoherence, Phys. Rep. **831**, 1 (2019).
[72] J. M. Raimond, M. Brune, and S. Haroche, Manipulating quantum entanglement with atoms and photons in a cavity, Rev. Mod. Phys. **73**, 565 (2001).
[73] To use a single parameter γ to adjust the relative strength, we assume that B and C have the same operator norm.
[74] W. F. Stinespring, Positive functions on C*-Algebras, Proc. Am. Math. Soc. **6**, 211 (1955).
[75] J. Novotný, G. Alber, and I. Jex, Asymptotic evolution of random unitary operations, Open Phys. **8**, 1001 (2010).
[76] K. M. R. Audenaert and S. Scheel, On random unitary channels, New J. Phys. **10**, 023011 (2008).
[77] M. Bauer and D. Bernard, Convergence of repeated quantum nondemolition measurements and wave-function collapse, Phys. Rev. A **84**, 044103 (2011).
[78] E. Haapasalo, T. Heinosaari, and Y. Kuramochi, Saturation of repeated quantum measurements, J. Phys. A: Math. Theor. **49**, 33LT01 (2016).
[79] W.-L. Ma, P. Wang, W.-H. Leong, and R.-B. Liu, Phase transitions in sequential weak measurements, Phys. Rev. A **98**, 012117 (2018).
[80] W.-L. Ma, S.-S. Li, and R.-B. Liu, Sequential generalized measurements: Asymptotics, typicality, and emergent projective measurements, Phys. Rev. A **107**, 012217 (2023).
[81] W. Yang, W.-L. Ma, and R.-B. Liu, Quantum many-body theory for electron spin decoherence in nanoscale nuclear spin baths, Rep. Prog. Phys. **80**, 016001 (2017).
[82] P. Szańkowski, G. Ramon, J. Krzywda, D. Kwiatkowski, and Ł. Cywiński, Environmental noise spectroscopy with qubits subjected to dynamical decoupling, J. Phys.: Condens. Matter **29**, 333001 (2017).
[83] G.-Q. Liu, X.-Y. Pan, Z.-F. Jiang, N. Zhao, and R.-B. Liu, Controllable effects of quantum fluctuations on spin free-induction decay at room temperature, Sci. Rep. **2**, 432 (2012).
[84] F. Reinhard, F. Shi, N. Zhao, F. Rempp, B. Naydenov, J. Meijer, L. T. Hall, L. Hollenberg, J. Du, R.-B. Liu, and J. Wrachtrup, Tuning a spin bath through the quantum-classical transition, Phys. Rev. Lett. **108**, 200402 (2012).
[85] M. B. Plenio and P. L. Knight, The quantum-jump approach to dissipative dynamics in quantum optics, Rev. Mod. Phys. **70**, 101 (1998).
[86] T. A. Brun, A simple model of quantum trajectories, Am. J. Phys. **70**, 719 (2002).
[87] C.-D. Qiu, Y.-D. Jin, J. -X. Zhang, G.-Q. Liu, and W.-L Ma, How coherence measurements of a qubit steer its quantum environment (unpublished).
[88] F. Wudarski, Y. Zhang, and M. I. Dykman, Nonergodic measurements of qubit frequency noise, Phys. Rev. Lett. **131**, 230201 (2023).
[89] M. W. Doherty, F. Dolde, H. Fedder, F. Jelezko, J. Wrachtrup, N. B. Manson, and L. C. L. Hollenberg, Theory of the ground-state spin of the NV^- center in diamond, Phys. Rev. B **85**, 205203 (2012).
[90] N. Zhao, S.-W. Ho, and R.-B. Liu, Decoherence and dynamical decoupling control of nitrogen vacancy center electron spins in nuclear spin baths, Phys. Rev. B **85**, 115303 (2012).
[91] L. Viola, E. Knill, and S. Lloyd, Dynamical decoupling of open quantum systems, Phys. Rev. Lett. **82**, 2417 (1999).
[92] C. A. Ryan, J. S. Hodges, and D. G. Cory, Robust decoupling techniques to extend quantum coherence in diamond, Phys. Rev. Lett. **105**, 200402 (2010).
[93] W.-L. Ma and R.-B. Liu, Angstrom-resolution magnetic resonance imaging of single molecules via wave-function fingerprints of nuclear spins, Phys. Rev. Appl. **6**, 024019 (2016).
[94] R. Blume-Kohout, H. K. Ng, D. Poulin, and L. Viola, Characterizing the structure of preserved information in quantum processes, Phys. Rev. Lett. **100**, 030501 (2008).
[95] R. Blume-Kohout, H. K. Ng, D. Poulin, and L. Viola, Information-preserving structures: A general framework for quantum zero-error information, Phys. Rev. A **82**, 062306 (2010).
[96] See proposition 6.2 in [58].